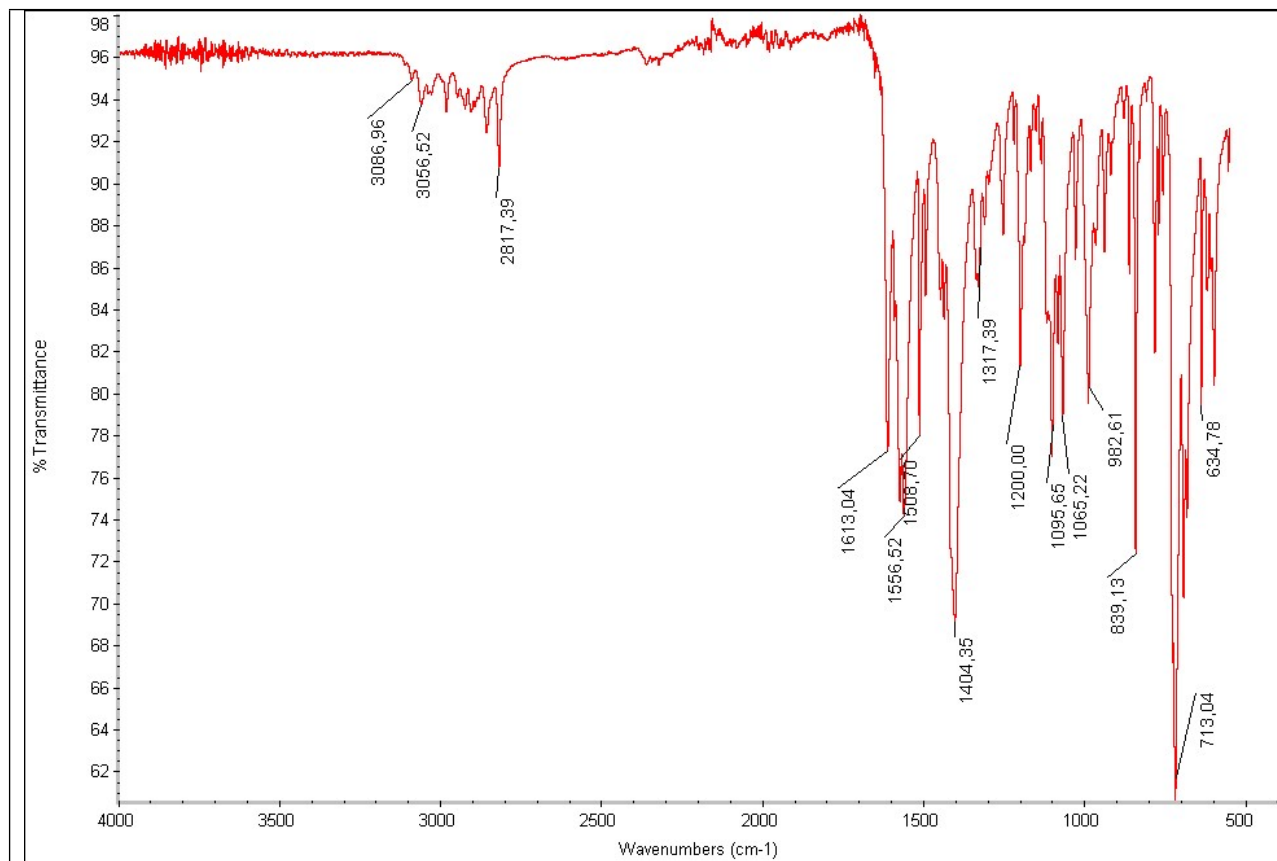


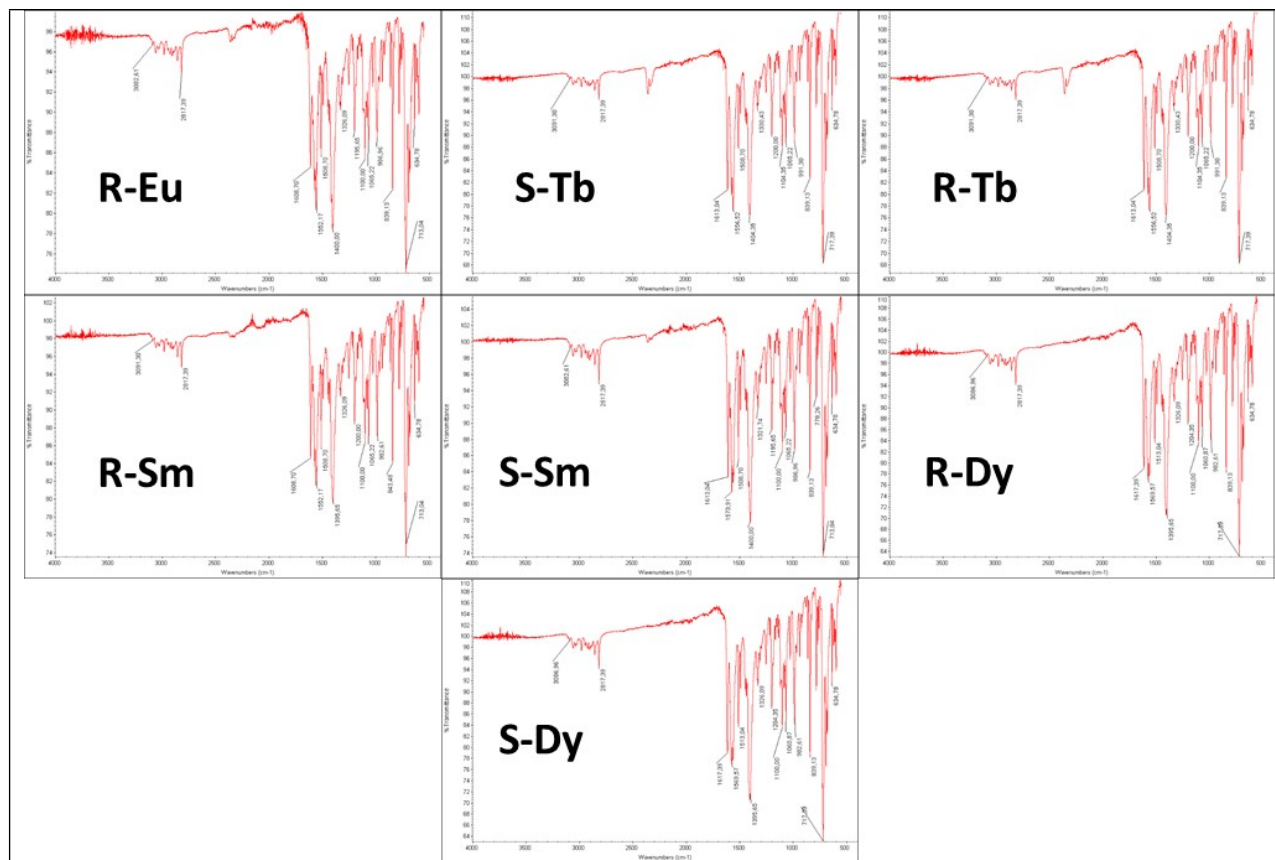
## Luminescence, CPL and magnetic properties on 1D enantiopure Ln<sup>3+</sup> complexes with (*S*-) and (*R*-) $\alpha$ -Methoxyphenylacetate Ligand.

Ànnia Tubau, Francesco Zinna, Lorenzo Di Bari, Mercè Font-Bardía and Ramon Vicente

### SUPPORTING INFORMATION:

#### INFRARED SPECTRA:



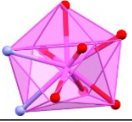
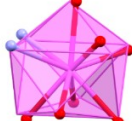
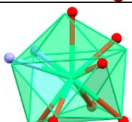
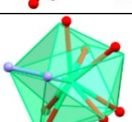
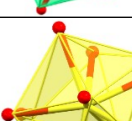
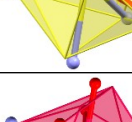


**Figure S1.** Infrared spectrum of compound **S-Eu** (top) and **R-Eu** to **S-Dy** (small figures, bottom). The samples were dispersed in a KBr pellet to perform de measurement.

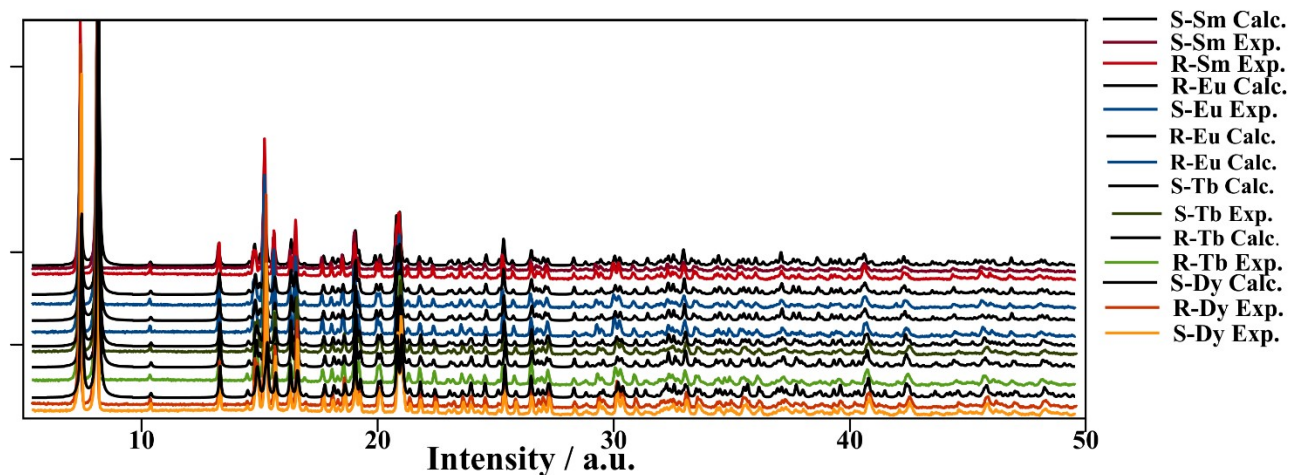
**STRUCTURE CHARACTERIZATION:**

<b>Crystal Data</b>	<b><i>R</i>-Eu</b>	<b><i>S</i>-Eu</b>	<b><i>R</i>-Tb</b>	<b><i>S</i>-Tb</b>	<b><i>S</i>-Dy</b>	<b><i>S</i>-Sm</b>
<b>Formula</b>	C <sub>39</sub> H <sub>35</sub> EuN <sub>2</sub> O <sub>9</sub>	C <sub>39</sub> H <sub>35</sub> EuN <sub>2</sub> O <sub>9</sub>	C <sub>39</sub> H <sub>35</sub> N <sub>2</sub> O <sub>9</sub> Tb	C <sub>39</sub> H <sub>35</sub> N <sub>2</sub> O <sub>9</sub> Tb	C <sub>39</sub> H <sub>35</sub> DyN <sub>2</sub> O <sub>9</sub>	C <sub>39</sub> H <sub>35</sub> N <sub>2</sub> O <sub>9</sub> Sm
<b>FW [g/mol]</b>	827.65	827.65	834.61	834.61	838.19	826.04
<b>Crystal System</b>	monoclinic	monoclinic	monoclinic	monoclinic	monoclinic	Monoclinic
<b>Space Group</b>	P21	P21	P21	P21	P21	P21
<b>a [Å]</b>	6.0481(3)	6.0472(3)	6.0348(3)	6.0361(3)	6.0246(2)	6.0523(2)
<b>b [Å]</b>	23.7053(12)	23.7026(11)	23.6379(12)	23.618(1)	23.5732(10)	23.7820(9)
<b>c [Å]</b>	12.2981(6)	12.3102(6)	12.3125(7)	12.3265(5)	12.3531(5)	12.2968(4)
<b>α [deg]</b>	90	90	90	90	90	90
<b>β [deg]</b>	100.971(2)	100.945(2)	101.130(2)	100.962(2)	101.095(2)	101.027(1)
<b>γ [deg]</b>	90	90	90	90	90	90
<b>V [Å<sup>3</sup>]</b>	1730.98(15)	1732.38(15)	1723.34(16)	1725.21(13)	1721.59(12)	1737.27(10)
<b>Z</b>	2	2	2	2	2	2
<b>T(K)</b>	100	100	100	100	100	100
<b>λ(Mo Kα) (Å)</b>	0.71073	0.71073	0.71073	0.71073	0.71073	0.71073
<b>D<sub>calc</sub> [g cm<sup>-3</sup>]</b>	1.588	1.587	1.608	1.607	1.617	1.579
<b>μ(Mo Kα) [mm<sup>-1</sup>]</b>	1.872	1.870	2.112	2.110	2.231	1.750
<b>R</b>	0.0394	0.0320	0.0118	0.0259	0.0308	0.0179
<b>wR<sub>2</sub></b>	0.0817	0.0614	0.0281	0.0575	0.0736	0.0405
<b>Flack x</b>	-0.002(7)	0.006(4)	0.002(3)	0.019(9)	0.018(15)	0.008(3)

**Table S1.** Crystallographic information from the single crystal X-Ray Diffraction measurements of compounds ***R/S*-Eu**, ***R/S*-Tb**, ***S*-Dy** and ***S*-Sm**

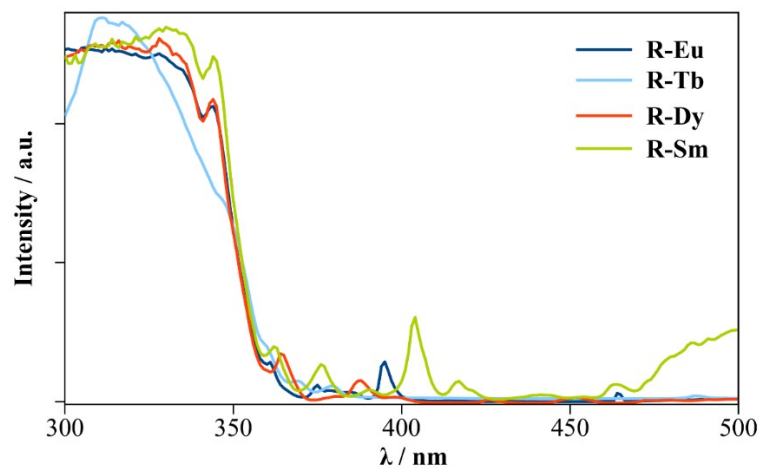
<i>Compound</i>	<b>TCTPR-9</b> (D <sub>3h</sub> )	CSAPR-9 (C <sub>4v</sub> )	MFF-9 (Cs)	
<b><i>R-Eu</i></b>	1.821	2.084	2.075	
<b><i>S-Eu</i></b>	1.928	2.129	2.166	
<b><i>R-Tb</i></b>	1.821	2.084	2.075	
<b><i>S-Tb</i></b>	1.832	2.088	2.097	
<b><i>S-Dy</i></b>	1.77501	2.07285	2.01299	
<b><i>S-Sm</i></b>	1.99236	2.15610	2.19200	

**Table S2.** Continuous Shape measurements (CShM) obtained for the coordination geometry of compounds ***R/S-Eu***, ***R/S-Tb***, ***S-Dy*** and ***S-Sm***. The calculation was done using the SHAPE program.

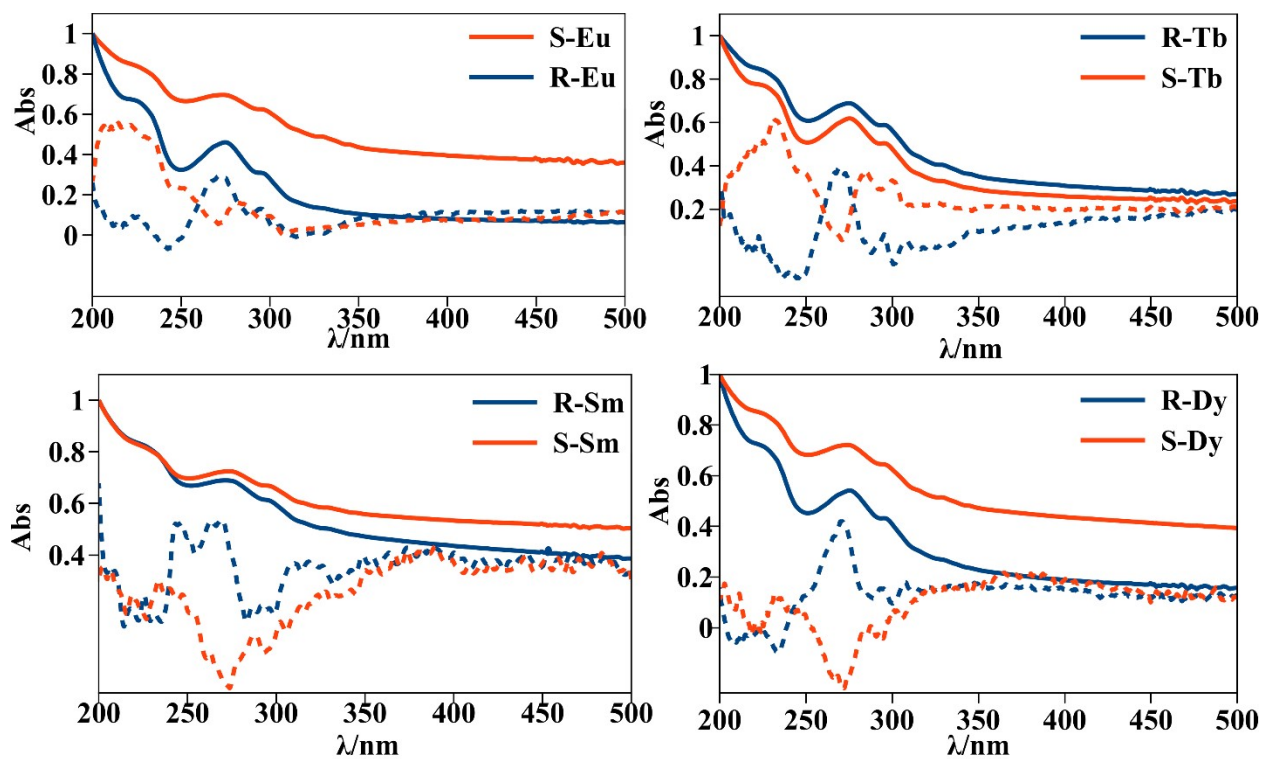


**Figure S2.** Powder X-Ray Diffraction (PDRX) of all the polycrystalline samples. The PDRX spectra of the polycrystalline samples were compared with the simulated PDRX spectra from the structures obtained by monocrystal X-Ray Diffraction.

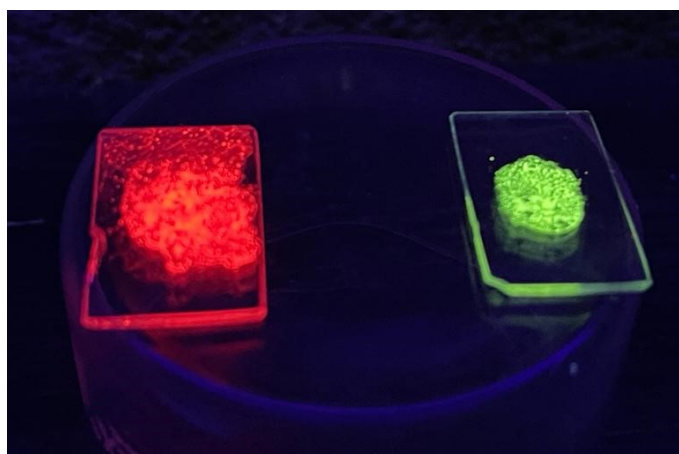
## OPTICAL PROPERTIES



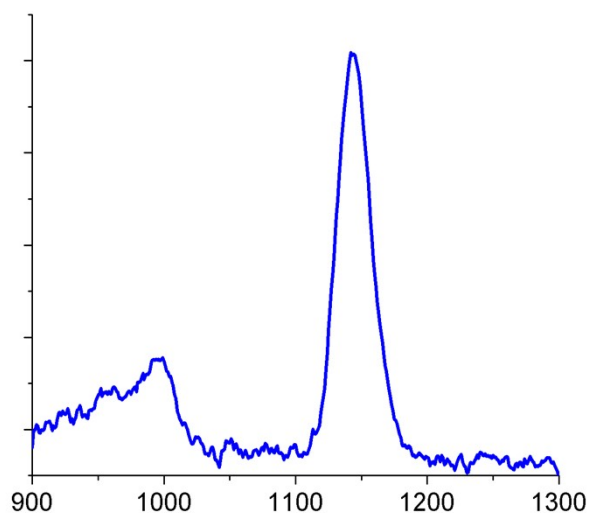
**Figure S3.** Excitation spectra for the *R*-enantiomers of the presented compounds.



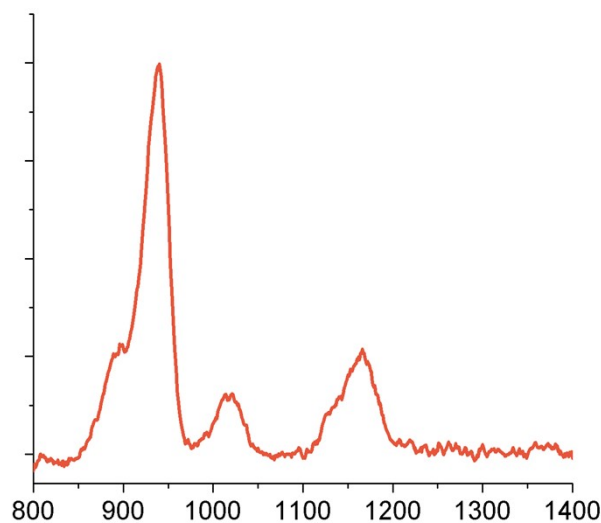
**Figure S4.** Solid state absorption of compounds *S/R*-Eu, Tb, Sm and Dy from the compounds dispersed in the KBr pellets. The Absorption spectra is compared with the Circular Dichroism spectra.



**Figure S5.** Emission color observed in the naked eye of compounds *R*-Eu and *R*-Tb under the radiation of a UV lamp.



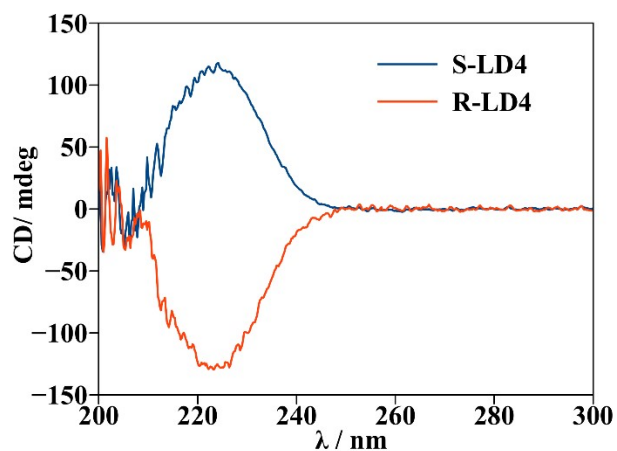
**Figure S6.** n-IR emission of compound **R-Dy** recorded at a  $\lambda_{exc}$  of 330 nm



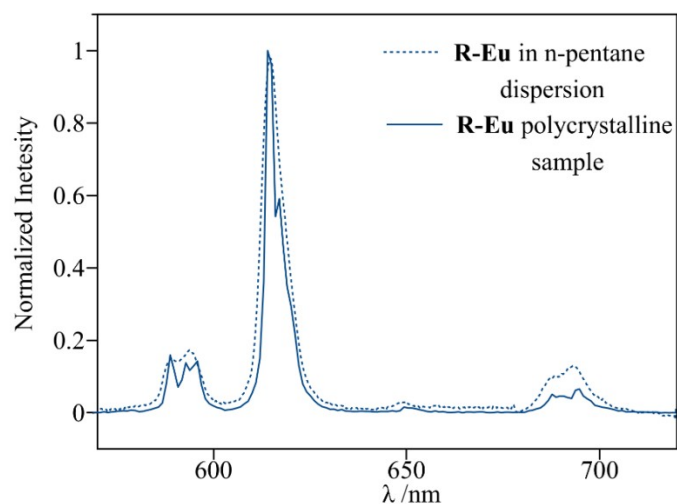
**Figure S7.** n-IR emission of compound **R-Sm** recorded at a  $\lambda_{exc}$  of 330 nm

$$\frac{1}{\tau_{rad}} = A_{MD,0} n^3 \left( \frac{I_{TOT}}{I_{MD}} \right) \quad (\text{Eq. S1})$$

Eq.S1.  $A_{MD,0}$  is a constant ( $14.65 \text{ cm}^{-1}$ ),  $n$  is the refractive index (1.517 for microcrystalline sample) and  $\frac{I_{TOT}}{I_{MD}}$  is the ratio between the total integrated area measured from the corrected Eu(III) emission spectrum ( $I_{TOT}$ ) to the integrated area of the pure magnetic dipole transition  ${}^5D_0 \rightarrow {}^7F_1$  ( $I_{MD}$ ).

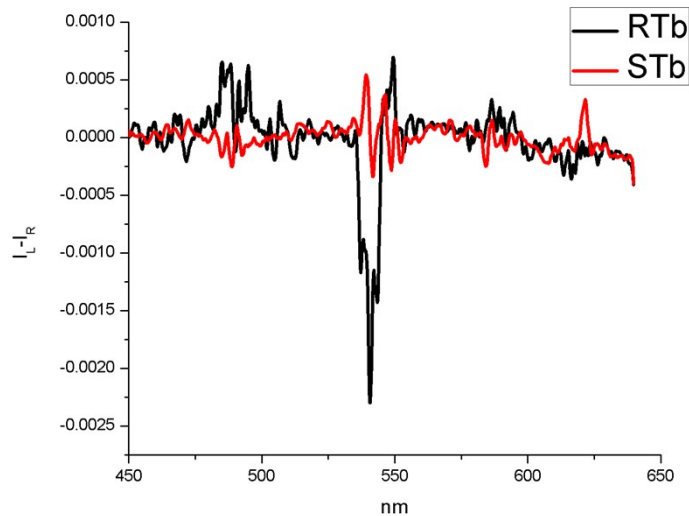


**Figure S8.** Circular Dichroism of the free (*R/S*)-(-)- $\alpha$ -Methoxyphenylacetic acid (*R/S*-HMPA) ligand. The respective samples were dissolved in ethanol solutions.



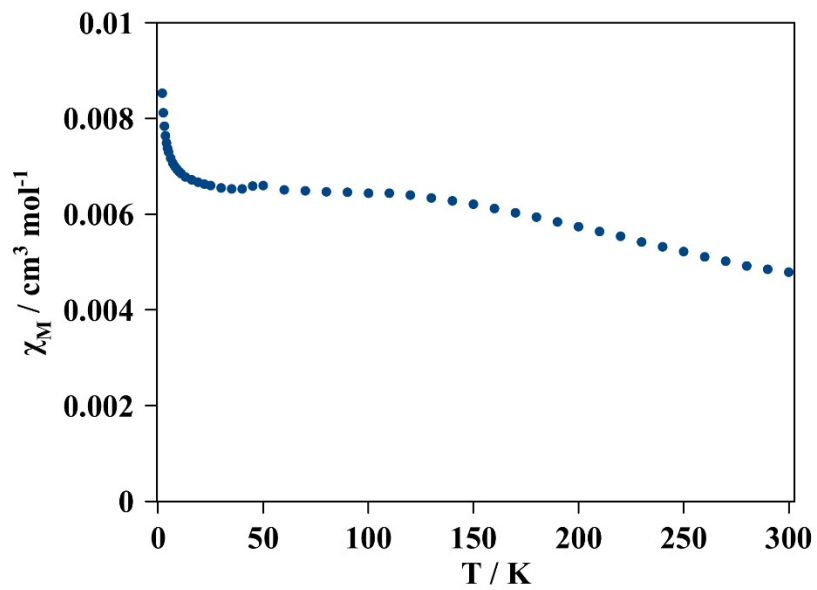
**Figure S9.** Emission spectra of compound **R-Eu** measured from the polycrystalline sample in a quartz plate (solid line) and the same polycrystalline sample dispersed in n-pentane in the quartz plate deposition (dashed line). The difference in the crystal field splitting that is differentiated in the polycrystalline sample is because the slits used in the different measurements were different and therefore, a change in the resolution of the spectra is observed. In the n-pentane dispersion the slits were 1mm and in the polycrystalline sample, the slits used were 0.3 nm.





**Figure S10.** CPL spectra of compounds *S/R*-Tb. The CPL signal was too weak to extract solid conclusions.

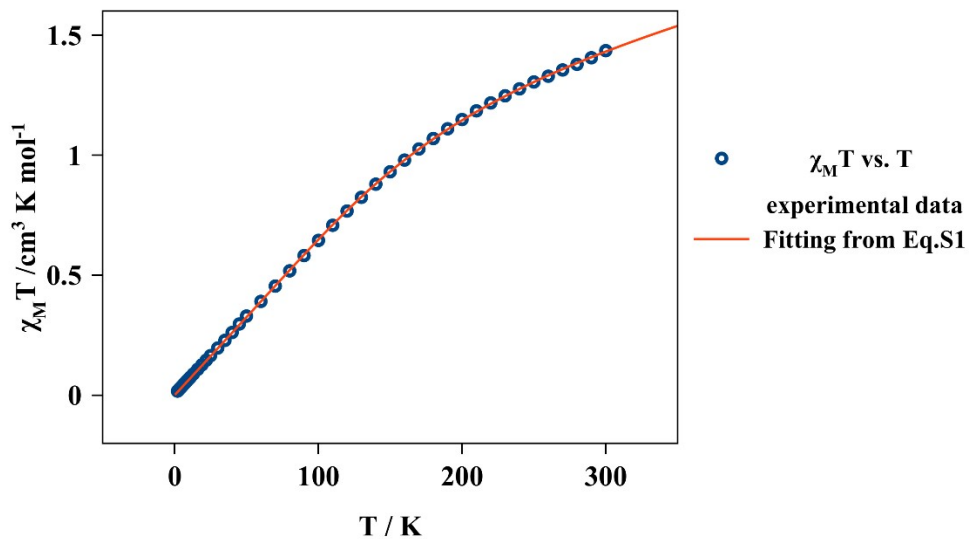
**MAGNETIC PROPERTIES:**



**Figure S11.**  $\chi_M T$  vs  $T$  plot for compound *S*-Eu.

$\chi_M T$ 

$$= \left( (N\beta^2/3kTx) [24 + (27x/2 - 3/2)e^{-x} + (135x/2 - 5/2)e^{-3x} + (189x - 7/2)e^{-6x} + (405x - 9/2)e^{-15x} + (2457x/2 - 13/2)e^{-21x}] / [1 + 3e^{-x} + 5e^{-3x} + 7e^{-6x} + 9e^{-10x} + 11e^{-15x} + 13e^{-21x}] \right) T$$

**Eq.S2**With  $x = \lambda/kT$ 

**Figure S12.**  $\chi_M T$  vs  $T$  plot for compound **S-Eu**. Red line corresponds to the best fitting using Eq.S1

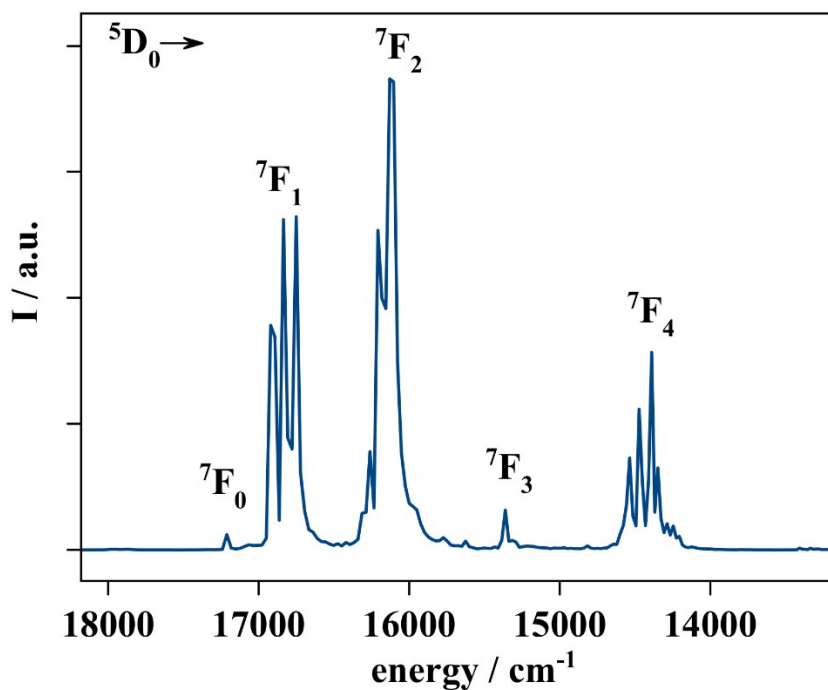


**Figure S13.** Emission spectra of compound **S-Eu** measured at 77K. The transition energies to  ${}^7F_0$  and  ${}^7F_1$  are depicted in the following table.

${}^5D_0 \rightarrow {}^7F_0$	17212
${}^5D_0 \rightarrow {}^7F_1$	16920 16835 16750
The transition energies are in $\text{cm}^{-1}$	

**Table S3.** The spin-orbit coupling parameter ( $\lambda$ ) is the energy gap between the  ${}^7F_0$  and  ${}^7F_1$  states. The three components arising from  ${}^7F_1$  transition due to crystal field are averaged. The resulting  $\lambda$  parameter is  $377 \text{ cm}^{-1}$  in agreement with the calculated from the magnetic data.

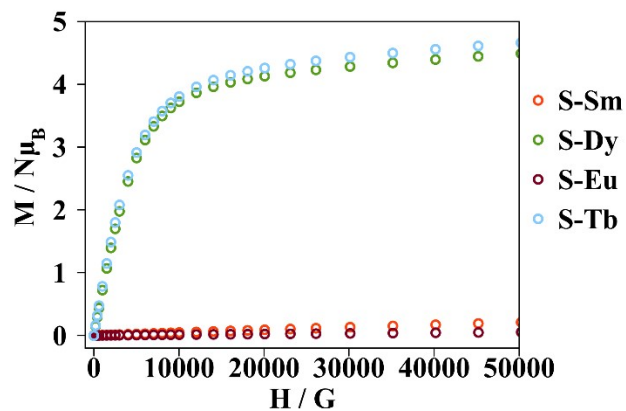


Figure S14. Magnetization dependence with external magnetic field measured at 2K.

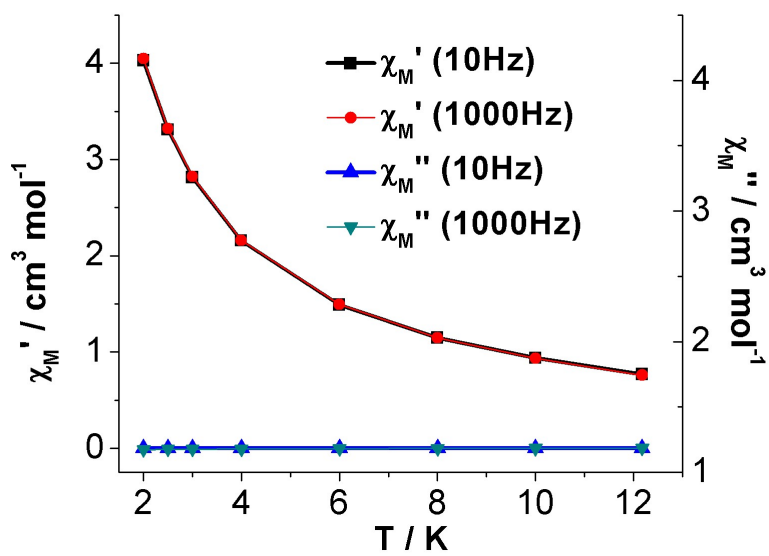
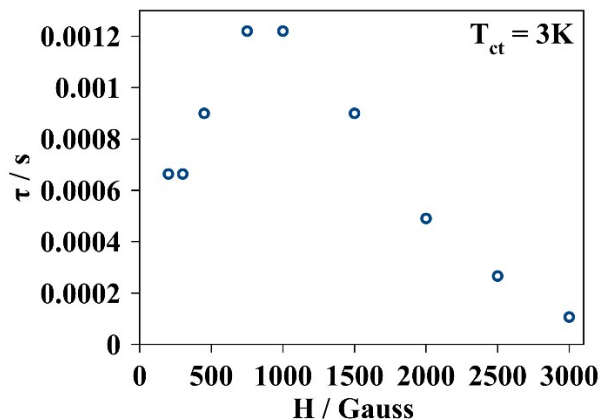
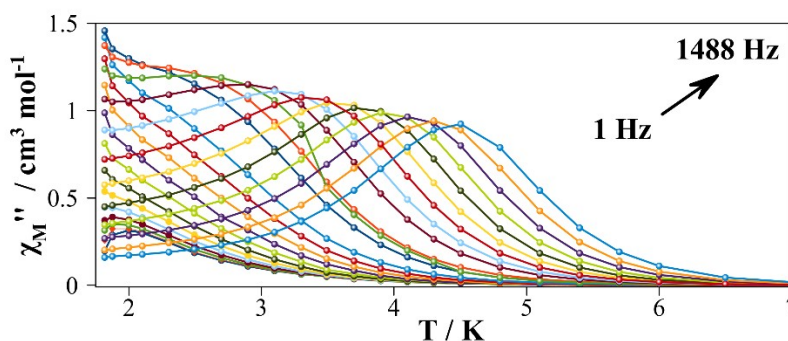


Figure S15. In-phase and out-of-phase magnetic susceptibility components, measured at a 0 dc magnetic field and an oscillating ac magnetic field of  $4 \cdot 10^{-4}$  T at 10 and 1000 Hz for compound **S-Dy**.



**Figure S16.** Relaxation times ( $1/2\pi\nu$ ) in front of different static magnetic fields measured at a constant temperature of 3K under an ac magnetic field of  $4 \cdot 10^{-4}$  T oscillating between 1 to 1488 Hz for **S-Dy**.



**Figure S17.** Temperature dependence of the out-of-phase magnetic susceptibility component ( $\chi_M''$ ). The experiment is measured under an external direct current magnetic field of 0.1 T and an altern current magnetic field of  $4 \cdot 10^{-4}$  T oscillating between 1 to 1488 Hz for **S-Dy**.

$$\chi_{AC}(\omega) = \chi_S + \frac{\chi_T - \chi_S}{1 + (i\omega\tau)^{(1-\alpha)}} \quad \text{Eq S3}$$

Generalized Debye model that describes a system with a distribution of the magnetization relaxation time. Where  $\chi_S$  and  $\chi_T$  are the adiabatic and thermal susceptibilities,  $\tau$  is the relaxation of the magnetization time and  $\omega$  is the angular frequency of the ac field ( $\omega = 1/2\pi f$ ).  $\chi_T$  is the susceptibility in the limit of the lowest field frequencies where the thermal equilibrium of the system is observed.  $\chi_S$  (lower than the  $\chi_T$ ) is observed when the oscillations of the ac field are fast compared to the time constant,  $\tau$ , and the magnetic system remains isolated from its environment. The  $\alpha$  parameter quantifies the width of the  $\tau$  distribution and it ranges from 0 to 1. The wider the distribution,  $\alpha$  acquires a larger value.

T/K	$\chi_s/\text{cm}^3 \text{ mol}^{-1}$	$\chi_T/\text{cm}^3 \text{ mol}^{-1}$	$\tau / \text{s}$	$\alpha$	residual
2.3	0.518711816	3.142314143	0.0024587061344742956	0.149953281	0.005335508
2.5	0.488352182	2.979170712	0.0020590740860810574	0.131165986	0.004223531
2.7	0.463543831	2.827393727	0.0016940170734923929	0.112316162	0.003311522
2.9	0.440876221	2.691452153	0.001363723260966314	0.096406489	0.002811319
3.1	0.420539991	2.564710189	0.001064967970415748	0.081647266	0.002550964
3.3	0.400452475	2.449262603	8.085337991977053E-4	0.070456784	0.003105104
3.5	0.386011933	2.335648927	5.987612681254692E-4	0.055788328	0.002505016
3.7	0.367686939	2.238769726	4.36478742829955E-4	0.048767035	0.002280816
3.9	0.348820841	2.14723514	3.126398140136009E-4	0.043148347	0.003039646
4.1	0.332269691	2.058807946	2.2298598812465294E-4	0.035739884	0.002292998
4.3	0.314343504	1.980330441	1.5874301089800148E-4	0.030055081	0.001920844
4.5	0.261721739	1.907163786	1.0663568618933868E-4	0.036535598	0.002804614
4.8	0.181169864	1.80244235	5.944910438224022E-5	0.032393284	0.002917499
5.1	0.022876753	1.70804243	3.1339853361623796E-5	0.02801976	0.003355619
5.4	0.012566339	1.622586665	1.8826031342289738E-5	0.002238009	0.013257982

**Table S4.** Relaxation parameters values for the best fit of  $\chi M''$  and  $\chi M'$  in front of frequency using the one component generalised Debye model for compound **S-Dy**.